Appl. Phys. B (2014) 117:731–735
DOI 10.1007/s00340-014-5888-9

Applied Physics B
Lasers and Optics

Nonlinear losses in photoconductive Yb:YAG laser materials: identification of photocarrier properties by non-steady-state photoEMF

N. Korneev · P. Rodriguez-Montero · U. Wolters · K. Petermann · G. Huber

Received: 27 February 2014 / Accepted: 20 June 2014 / Published online: 8 July 2014

Abstract We report on the investigation of the photocarrier sign and the excitation dynamics in Yb:YAG at 940 nm excitation wavelength by non-steady-state photoelectromotive force technique. Annealed crystals with 25 and 50 % Yb-doping concentration demonstrate hole conductivity, while 80 % Yb:YAG displays electron conductivity. A characteristic relaxation time of approximately 1 ms is observed, which corresponds to the lifetime of the excited Yb^{3+}-ion.

1 Introduction

Yb:YAG as a laser material offers a high doping potential, a low quantum defect and superior thermo-physical properties. The energy level structure of Yb^{3+} consists of only two 4f manifolds, for which energy transfer processes such as cross-relaxation and upconversion are not expected. Nevertheless, a decrease in laser efficiency of Yb:YAG thin-disk lasers with increasing inversion level has been reported [1]. These processes depend on the excitation density in the active medium and reduce the laser efficiency of Yb:YAG crystals at Yb-concentrations above 12 %. Similar observations have been made in ceramic Yb:YAG laser crystals [2] as well as in highly doped Yb:LuAG crystals [3]. Research has focussed on this surprising shortcoming, as there is a strong demand for higher output powers which require high doping and high inversion levels. In the course of this research, photoconductivity measurements have confirmed the creation of free charge carriers in Yb-doped single crystals when irradiated with pump light of 940 nm [4, 5]. A nonlinear increase of photocurrent with the excitation density was found, suggesting an energy transfer mechanism that involves two to three Yb^{3+}-excitations. The corresponding energy, though, is not sufficient for an electron to move across the host's band gap. Therefore, photocarrier generation in Yb:YAG laser crystals is linked to transient Yb^{2+}-ions in the crystal, which are created by a charge transfer process that forms transient Yb^{2+}-ions and O^{-}-ions. In the attempt to identify the mechanism underlying the nonlinear laser losses, the non-steady-state photoelectromotive force (photoEMF) technique has been found a suitable method to gain information on the photocarrier properties.

2 Methods

The non-steady-state photoEMF technique was developed for characterization of photorefractive crystals [6–10] and other photoconductors [11, 12]. If a sample is illuminated with an oscillating pattern of interference fringes, a moving photocarrier distribution and relatively stable space charge distribution corresponding to the average fringe position are created. Their interaction results in an alternating current that can be collected from the electrodes on the sample faces. The frequency dependence of current permits to determine carrier sign (or bipolar character), dielectric relaxation time and characteristic carrier lifetime. A review of the effect and its applications is given in [6].

N. Korneev · P. Rodriguez-Montero
Instituto Nacional de Astrofísica, Óptica y Electrónica, Apdo. Postal 51 y 216, CP 72000 Puebla, Mexico

U. Wolters (✉) · K. Petermann · G. Huber
Institut für Laser-Physik, Universität Hamburg, Luruper Chaussee 149, 22761 Hamburg, Germany
e-mail: uwolters@physnet.uni-hamburg.de

The sinusoidal displacement of the interference pattern from its average position is given by the expression $\Delta(t) = \Delta \sin(\Omega t)$ with the relative phase of the fringe pattern Δ, oscillation frequency Ω and time t. Some of the parameters that govern the complex amplitude of the photoEMF current density of a monopolar photoconductor are as follows: the fringe spacing Λ, the carrier diffusion length L_D, the characteristic time of space charge grating relaxation τ_{di} and the characteristic time of photoconductivity relaxation τ. The second characteristic time τ can physically correspond to a finite carrier lifetime, shallow trap dynamics or to the dynamics of photocurrent excitation.

For $L_D \ll \Lambda$ and a space charge relaxation time τ_{di} longer than the photoconductivity time constant τ, the photoEMF signal amplitude at low oscillation frequencies Ω grows proportionally to Ω up to the characteristic frequency τ_{di}^{-1}, it then remains nearly constant until Ω reaches the upper cutoff frequency τ^{-1} and diminishes for even higher frequencies. The signal phase changes by 180° from low to high frequencies. At the frequency Ω_{max} corresponding to the maximum of the current amplitude, the photoEMF phase relative to the phase of vibration is close to either 0° or 180°, depending on the sign of the photocarriers. If the space charge relaxation is faster than the photoconductivity relaxation, the two characteristic frequencies are interchanged. If there are two carriers present in the photoconductor, the behavior of the photoEMF signal as a function of frequency becomes more complicated, as discussed in [6–8] with respect to semiconductors.

2.1 Sample preparation and experimental setup

The interference fringes were created by superposition of two laser beams from the same source, a Ti:Sapphire laser with 940 nm continuous wave emission. The output beam was divided by a beam splitter. One beam was phase-modulated with an electro-optical modulator (EOM) producing a vibration amplitude of 1 rad, and the beams were individually focused with two lenses of 30 cm focal length. The beams crossed at an angle of 55° which corresponds to 1.2 μm fringe spacing at a wavelength of 940 nm. Maximum output power of the Ti:Sapphire laser at 940 nm was limited to below 600 mW and was further reduced for part of the measurement with neutral density filters. The photocurrent in the samples increases superlinearly with incident intensity [5], and reducing the spot diameter strongly enhances the photoEMF signal. To obtain a sufficient signal-to-noise ratio, the laser beams were focused to 300–400 μm spot diameter matching the interelectrode distance. Two electrode geometries, as depicted in Fig. 1, were used. Type 1 are bulk crystals of approximately $5 \times 5 \times 1$ mm size with two silver paste stripe electrodes deposited on the front surface spaced at a distance of about 0.3–0.5 mm.

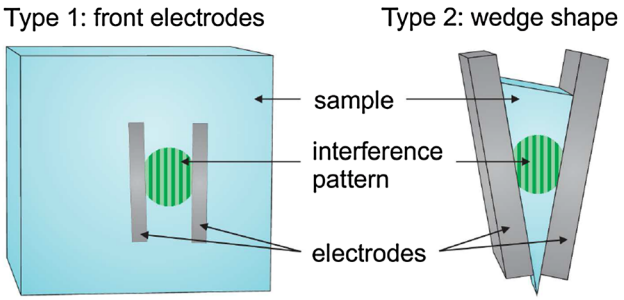

Fig. 1 Sample and illumination geometry. *Left* type 1 design with front electrodes (silver paint stripes). *Right* type 2 design with wedge shaped sample placed between two brass electrodes. The spacing of the interference fringes is enlarged for better visibility

Because the absorption length for 940 nm is small for highly doped samples, this geometry permits rather efficient collection of current. The type 2 sample had a wedge shape, with a triangular base that had two sides of approximately 5 mm and one side of 1 mm length and a sample thickness of 1.5 mm. The samples were fixed by silver paint to brass electrodes with an area of 0.5 cm^2 each which also offer an efficient heat removal. By focussing the incident light beams at different parts of the sample, different effective interelectrode distances can be chosen. The samples were placed inside an aluminum protective box and connected directly to a lock-in amplifier with a load resistor in the range of $M\,\Omega$. The measured current data were corrected for input capacitance. A dual phase lock-in amplifier was used to determine the amplitude of the photoEMF signal as well as the signal phase relative to the EOM modulating voltage. The electric setup including the EOM was calibrated using a BSO ($Bi_{12}SiO_{20}$) crystal, with green laser (532 nm, 50 mW) excitation. The results were consistent with those reported earlier in the literature [6, 10]. Since the carriers in BSO are known to be electrons, the measured electrical signal phase on the lock-in was used to fix the sign convention to a phase of 0° for electrons (−90° to +90°) and 180° for holes (90°–270°).

The investigated samples, fabricated at the Institute of Laser-Physics, were grown by the Czochralski technique from high-purity raw materials (5N) using 6N rhenium crucibles. The rhenium crucibles demand a reducing growth atmosphere, and the resulting crystals consequently contain a large amount of oxygen vacancies, which cause a characteristic blue color. Annealing at approximately 1,000 °C for several days eliminates the oxygen vacancies from the crystal, and samples suitable for laser operation are obtained. Table 1 gives an overview of the samples examined in this study.

In addition to the 25 % Yb:YAG samples in wedge shape, two corresponding samples from the same boule with front electrode geometry have been investigated. The results were consistent, but yielded 3–5 times smaller signal due to a worse collection of current. It is therefore

Table 1 Investigated Yb:YAG samples

	Sample	Shape
#1	25 % Yb:YAG	Wedge shaped, front electrodes
#2	50 % Yb:YAG	Wedge shaped
#3	80 % Yb:YAG	Front electrodes

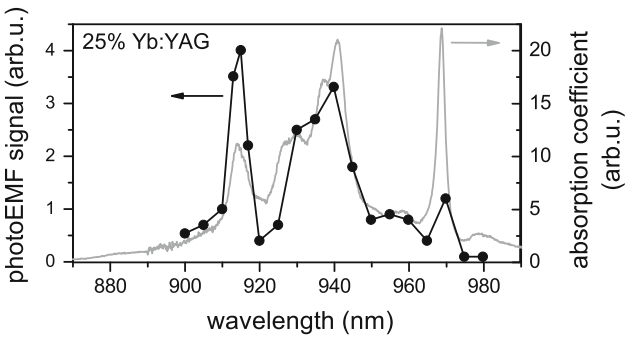

Fig. 2 Spectral dependence of photoEMF signal (*black dots*) for sample #2 (25 % Yb:YAG). The *curve* is obtained by manually changing the Ti:Sapphire wavelength. The photoEMF signal well corresponds to the Yb^{3+} absorption spectrum (*gray curve*)

confirmed that the different electrode configurations do not affect the general character of the current curves and that the 80 % Yb:YAG sample is fully comparable with the wedge-type samples.

3 Experimental results

The spectral dependencies of the photoEMF current amplitude for wavelengths in the range 900–980 nm are qualitatively similar for all investigated samples. The current is highest at wavelengths that correspond to the local absorption maxima of the Yb^{3+} absorption spectrum, as shown in Fig. 2. The peaks of the photoEMF signal increase with Yb-concentration. For all samples, a large signal is observed at 940 nm, and, thus, the experiments with different modulation frequencies Ω were conducted at this wavelength, which is also typical for laser pumping. The results are summarized in Table 2. A simple graphic procedure, as illustrated in Fig. 3, was used to estimate the characteristic times. This method is reliable as long as the two characteristic times are well separated, and no bipolar behavior, that is a mixed conductivity of electrons as well as holes, is observed.

3.1 25 and 50 % Yb:YAG

The dependence of the photoEMF current on the modulation frequency is qualitatively similar for the 25 % (#1) and 50 % Yb:YAG (#3) laser crystals. As shown in Fig. 3 for 25 % Yb:YAG, the signal phase changes from approximately

Table 2 Summary of the photoEMF results

Sample	Carrier type	Pump power (mW)	Characteristic time constants (ms)	
#1	Holes	370	20	**1.3**
		500	40	**1.3**
#2	Holes	305	4.5	**0.8**
		490	2.7	**0.9**
#3	Electrons	125	**1.2**	0.23
		500	**1.2**	0.16

Bold values correspond to the characteristic relaxation frequencies that match the $^{3+}$ lifetime

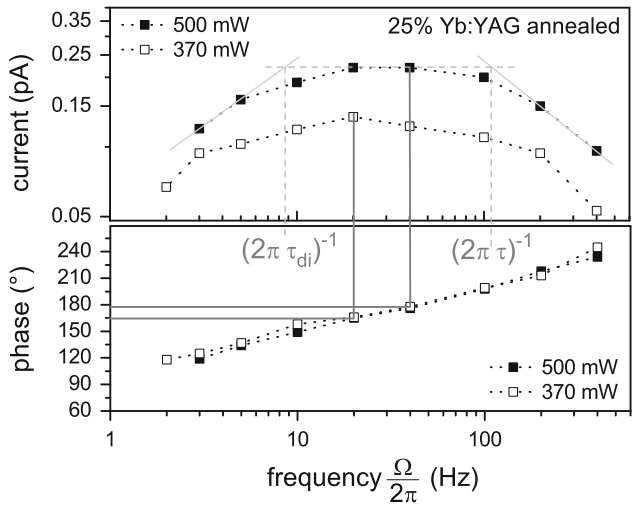

Fig. 3 PhotoEMF signal of 25 % Yb:YAG (sample #1) at different pump powers. The *vertical lines* mark the frequency Ω_{max} at maximum current amplitude, and the *horizontal lines* show the corresponding phase. Exemplarily, the *gray tangential lines* depict the graphical method (as explained in the text) to determine the two cutoff frequencies τ_{di} and τ [6]

90°–270° and is about 180° at the current maximum. The curve is characteristic for a single carrier with a relaxation process in photoconductivity, the carriers being well-defined holes. The high cutoff frequency is between 100 and 200 Hz for both samples and hardly changes with pump intensity. The lower cutoff is due to dielectric relaxation; it grows with higher intensities. Figure 4 shows the results obtained for 50 % Yb:YAG. At comparable pump intensity, the lower cutoff frequency is approximately one order of magnitude larger in the 50 % Yb-doped sample than at 25 % Yb-doping, which reflects again a predominant hole conductivity.

3.2 80 % Yb:YAG

In the sample with the highest doping concentration investigated in this series (#3), the signal is electron-dominated and no big influence of holes is seen (Fig. 5). Here, the dielectric cutoff frequency is higher than the

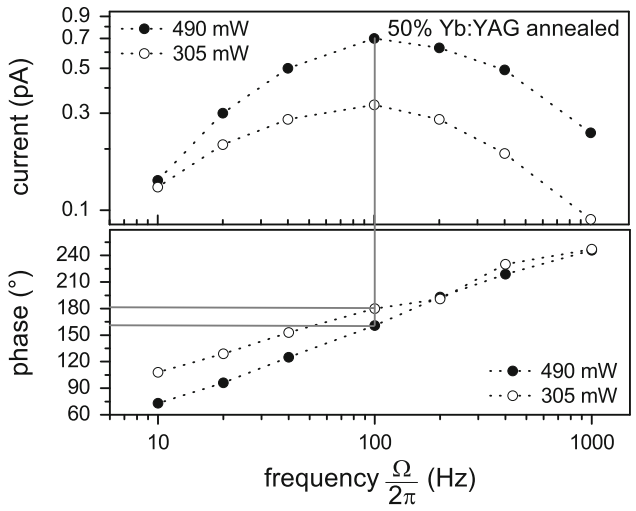

Fig. 4 PhotoEMF signal of 50 % Yb:YAG (sample #2) at different pump powers. The phase shift at maximum current amplitude indicates hole conductivity

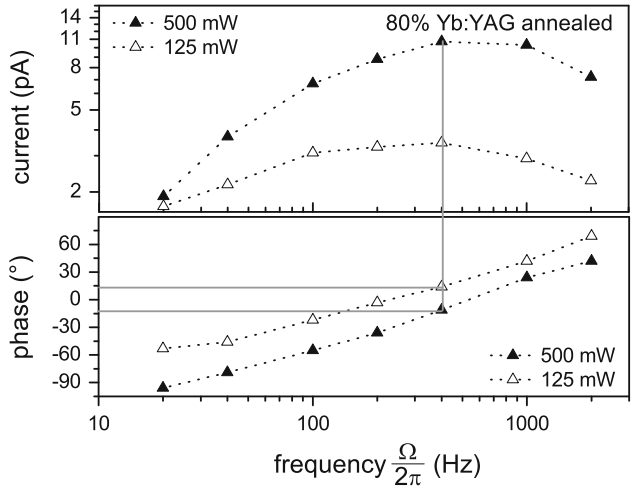

Fig. 5 PhotoEMF signal of 80 % Yb:YAG (sample #3) at different pump powers. The phase shift at maximum current amplitude indicates electron conductivity

photoconductivity relaxation one. The signal amplitudes and cutoff frequencies are both rather high, reflecting the high photoconductivity of this sample.

4 Discussion and conclusion

The photoEMF measurement is a useful technique to determine the photocarrier sign and dynamics in Yb-doped YAG crystals. Different from most materials investigated so far with this method, tightly focused high-power beams are necessary to obtain a good signal-to-noise ratio. Due to the non-uniform illumination, the exact fitting by a theoretical expression is complicated and the curves are interpreted qualitatively, yielding the results summarized in Table 2. The behavior of the 25 and 50 % Yb:YAG laser samples is well described by a one carrier model with hole conductivity. In 80 % Yb:YAG, electron conductivity is observed. The creation of different carriers in the different samples suggests that the Yb^{3+}-concentration strongly influences the Yb:YAG photoconductivity behavior.

As demonstrated in [5], the photocurrent created in Yb:YAG increases nonlinearly with pump power, showing exponents of two to three. This indicates that a number of two to three excited Yb^{3+}-ions are involved in the process. The results presented here provide a further insight into the mechanism of photocarrier creation, which for typical laser crystals with low to medium doping concentration is the generation of holes. In a tentative model, it is presumed that several excited Yb^{3+}-ions relax simultaneously and release sufficient energy to transfer an electron from a nearby oxygen ligand to an Yb^{3+}-ion, forming a transient Yb^{2+}-ion. The hole at the oxygen ligand is then excited into the valence band, i.e., by photon absorption, which gives rise to the observed hole conductivity. The spectroscopic identification of the transient Yb^{2+} as well as O^{-}-centers created in the process is the aim of further research. Once a critical density of Yb^{3+}-ions is reached, that is in crystals with doping concentrations above 50 %, electron conductivity dominates. This is possible if due to the described charge transfer a high density of transient Yb^{2+}-ions is created to allow for an electron hopping conductivity between the doped Yb-ions. Unfortunately, it is not feasible to determine the transition point between hole and electron conductivity with the qualitative photoEMF analysis used in this work, as it is not applicable in the case of bipolar behavior.

A characteristic relaxation frequency of 100–200 Hz is found for all investigated samples at different excitation levels. This frequency approximately corresponds to the lifetime of 1 ms of the excited Yb^{3+}-ions (see bold figures in Table 2), confirming the Yb^{3+}-excitation to be the fundamental process for photocarrier generation.

The presented results allow a better understanding of the nonlinear losses observed in highly Yb-doped thin-disk lasers. The proposed mechanism implies a severe loss of Yb^{3+} excitation energy, which strongly increases the pump power necessary to reach threshold inversion and obtain laser operation. Furthermore, the absorption of the laser radiation by the created photocarriers imposes an additional laser loss. While these effects apply to Yb:YAG lasers in general, thin-disk laser media which require particularly high excitation densities are especially prone to inversion dependent losses. Hence, the creation of holes by Yb^{3+} excitation energy accounts for the low slope efficiency of Yb:YAG thin-disk lasers observed at high output coupling transmissions and high doping concentrations.

References

1. M. Larionov, K. Schuhmann, J. Speiser, C. Stolzenburg, A. Giesen, in *Advances Solid-State Photonics 98 in OSA Trends in Optics and Photonics*, Paper 18 (2005)
2. A. Pirri, G. Toci, D. Alderighi, M. Vannini, Opt. Express **18**, 17262 (2010)
3. A. Pirri, G. Toci, M. Nikl, V. Babin, M. Vannini, Opt. Express **22**, 4038 (2014)
4. J.F. Bisson, D. Kouznetsov, K.I. Ueda, S.T. Fredrich-Thornton, K. Petermann, G. Huber, Appl. Phys. Lett. **90**, 201901 (2007)
5. C. Brandt, S.T. Fredrich-Thornton, K. Petermann, G. Huber, Appl. Phys. B **102**, 765–768 (2011)
6. S. Stepanov, in *Handbook of Advanced Electronic and Photonic Materials and Devices*, ed. by H.S. Nalwa (Academic Press, New York, 2001), pp. 205–272
7. N.A. Korneev, S. Mansurova, S. Stepanov, JOSA B **12**, 615–620 (1995)
8. N.A. Korneev, S. Mansurova, S. Stepanov, J. Appl. Phys. **78**, 2925 (1995)
9. M.P. Petrov, I.A. Sokolov, S.I. Stepanov, G.S. Trofimov, J. Appl. Phys. **68**, 2216 (1990)
10. I.A. Sokolov, S.I. Stepanov, Electron. Lett. **26**, 1275 (1990)
11. G.S. Trofimov, A.I. Kosarev, A.G. Kovrov, P.G. LeComber, J. Non-Cryst, Solids **137–138**, 483–486 (1991)
12. R. Bittner, K. Meerholz, S. Stepanov, Appl. Phys. Lett. **74**, 3723 (1999)